Hyeon-Ju Jeong,[1] Hye-Jin Lee,[1] Tuan Anh Vuong,[1] Kyu-Sil Choi,[2] Dahee Choi,[3] Sung-Hoi Koo,[3] Sung Chun Cho,[4] Hana Cho,[5] and Jong-Sun Kang[1]

Prmt7 Deficiency Causes Reduced Skeletal Muscle Oxidative Metabolism and Age-Related Obesity

Diabetes 2016;65:1868–1882 | DOI: 10.2337/db15-1500

Downloaded from http://diabetesjournals.org/diabetes/article-pdf/65/7/1868/599654/db151500.pdf by guest on 21 April 2025

METABOLISM

Maintenance of skeletal muscle function is critical for metabolic health and the disruption of which exacerbates many chronic diseases such as obesity and diabetes. Skeletal muscle responds to exercise or metabolic demands by a fiber-type switch regulated by signaling-transcription networks that remains to be fully defined. Here, we report that protein arginine methyltransferase 7 (Prmt7) is a key regulator for skeletal muscle oxidative metabolism. Prmt7 is expressed at the highest levels in skeletal muscle and decreased in skeletal muscles with age or obesity. *Prmt7*$^{-/-}$ muscles exhibit decreased oxidative metabolism with decreased expression of genes involved in muscle oxidative metabolism, including PGC-1α. Consistently, *Prmt7*$^{-/-}$ mice exhibited significantly reduced endurance exercise capacities. Furthermore, *Prmt7*$^{-/-}$ mice exhibit decreased energy expenditure, which might contribute to the exacerbated age-related obesity of *Prmt7*$^{-/-}$ mice. Similarly to *Prmt7*$^{-/-}$ muscles, Prmt7 depletion in myoblasts also reduces PGC-1α expression and PGC-1α–promoter driven reporter activities. Prmt7 regulates PGC-1α expression through interaction with and activation of p38 mitogen-activated protein kinase (p38MAPK), which in turn activates ATF2, an upstream transcriptional activator for PGC-1α. Taken together, Prmt7 is a novel regulator for muscle oxidative metabolism via activation of p38MAPK/ATF2/PGC-1α.

With skeletal muscle aging (called sarcopenia), one exhibits decreased muscle mass and exercise capacities accompanied by increased fatigability and muscle atrophy leading to a reduced quality of life (1–3). Skeletal muscle exhibits a remarkable plasticity in energy metabolism and contractile functions in response to various stimuli like exercise, hormones, or nutritional states (4). Defects in the oxidative metabolism and function of skeletal muscle have been implicated in numerous metabolic pathologies, including insulin resistance, glucose intolerance, and obesity (5–8). Skeletal muscle adaptation toward oxidative metabolism promoted by stimuli like endurance exercise involves multiple signaling pathways, including Ca2+/calmodulin-dependent protein kinases, AMPKs, and p38 mitogen-activated protein kinase (p38MAPK), which induce the expression and activation of a key transcriptional coactivator, PGC-1α (9–13). PGC-1α is a critical regulator for mitochondrial function and oxidative muscle metabolism (9,14,15). Consistently, mice lacking PGC-1α exhibit declined muscle oxidative metabolism and exercise capacity (16,17). Furthermore, PGC-1α expression in skeletal muscle is reduced in obesity, diabetes, or denervation associated with the fiber-type switch toward glycolytic fibers (15,18–21). PGC-1α is preferentially expressed in oxidative fibers, and its ectopic expression in skeletal muscle drives oxidative fiber formation, at least in part through MEF2 interactions thereby directly activating oxidative fiber-specific gene expression (22). Among signaling pathways, p38MAPK (p38) plays a critical role for metabolic adaptations of skeletal muscle induced by exercise-triggered muscle contraction, which is mediated

[1]Department of Molecular Cell Biology, Sungkyunkwan University School of Medicine, Samsung Biomedical Research Institute, Suwon, South Korea
[2]Samsung Biomedical Research Institute, Samsung Medical Center, Seoul, South Korea
[3]Division of Life Science, Korea University, Seoul, South Korea
[4]Well Aging Research Center, Samsung Advanced Institute of Technology, Samsung Electronics Co. Ltd., Suwon, South Korea
[5]Department of Physiology, Sungkyunkwan University School of Medicine, Samsung Biomedical Research Institute, Suwon, South Korea

Corresponding author: Jong-Sun Kang, kangj01@skku.edu.

Received 30 October 2015 and accepted 19 April 2016.

This article contains Supplementary Data online at http://diabetes.diabetesjournals.org/lookup/suppl/doi:10.2337/db15-1500/-/DC1.

H.-J.J. and H.-J.L. contributed equally to this study.

© 2016 by the American Diabetes Association. Readers may use this article as long as the work is properly cited, the use is educational and not for profit, and the work is not altered.

through regulation of PGC-1α expression and activity. p38 can phosphorylate the transcription factors, such as ATF2 and MEF2c, to stimulate the transcription of the PGC-1α gene (23–25). In addition, p38 can derepress PGC-1α by phosphorylation and in turn PGC-1α can autoregulate via interaction with MEF2c (24,26). The ectopic activation of p38 by expression of a constitutive active form of MAPK kinase 6 (MKK6EE) enhanced oxidative metabolism by the upregulation of PGC-1α and mitochondrial proteins in skeletal muscles (24). ATF2 binds to the CRE (cAMP response element) sequence in the PGC-1α promoter region in addition to CREB transcription factors to stimulate gene expression (23,24). Recent studies suggest the cross talk and redundancy of signaling pathways aforementioned in regulation of fiber-type switch and oxidative metabolism in response to exercise. Even though PGC-1α was long believed to be indispensible for the muscle adaptation in response to exercise (27,28), mice lacking PGC-1α still showed the exercised-induced fiber-type switch with the reduced expression of mitochondrial genes, suggesting that PGC-1α is specifically required for mitochondrial function involved in muscle adaptation (29). These studies suggest that the signaling-transcription network promoting skeletal muscle adaptation induced by various stimuli including exercise remains to be fully defined.

Protein arginine methyltransferases (Prmts) catalyze symmetric or asymmetric dimethylations of arginine residues on both histone and nonhistone substrates linked to gene regulation in diverse biological processes including glucose metabolism and myoblast differentiation (30,31). Based on dimethylation characteristics, Prmts can be classified as either the type I catalyzing asymmetric arginine dimethylation (Prmt1, Prmt2, Prmt3, Prmt4, Prmt6, Prmt8) or the type 2 subfamily generating symmetric dimethylarginine residues (Prmt5 and Prmt7) (30,32). Among these, Prmt1, -4, and -5 are relatively well studied and known to play critical roles in various biological processes. Recent studies have shown that Prmt1 and Prmt5 are involved in regulation of hepatic gluconeogenesis through inhibition of FOXO (33) or through activation of CREB (34). In addition, Prmt1 has been shown to methylate PGC-1α and thereby stimulates the nuclear receptor–mediated expression of mitochondrial genes in nonmuscle cells (35). Prmt4 and Prmt5 have been implicated in promotion of myoblast differentiation through interaction with Mef2c or MyoD, respectively (36,37). Recent studies with muscle stem cell–specific knockout mouse models have suggested that Prmt4 and Prmt5 play critical roles in control of muscle stem cell functions during muscle regeneration (38,39). In this study, we characterized the role of Prmt7 in skeletal muscle metabolism by using Prmt7-deficient mouse models. Prmt7 is highly expressed in skeletal muscle, and its expression declines in skeletal muscles with age and obesity. Interestingly, Prmt7 deficiency results in reduced oxidative metabolism and diminished endurance exercise capacity. Furthermore, Prmt7-deficient mice exhibit age-related obesity with excessive body fat accumulation and hyperglycemia. This function of Prmt7 appears to be partly mediated through regulation of PGC-1α expression by interaction with and activation of p38. Taken together, our data support that Prmt7 is important for muscle function maintenance, thereby contributing to balanced body metabolism.

RESEARCH DESIGN AND METHODS

Animal Studies

Male and female Prmt7$^{<tm1a(EUCOMM)Wtsi>}$ mice were purchased from the Sanger Institute. All animal experiments were approved by the Institutional Animal Care and Research Advisory Committee at Sungkyunkwan University School of Medicine Laboratory Animal Research Center. Mice were backcrossed onto C57BL/6J background for at least six generations and maintained on C57BL/6J background, and littermate wild-type controls were used for comparison with *Prmt7*$^{-/-}$ mice in all experiments. To assess the age-related effect of Prmt7 deficiency on obesity, *Prmt7*$^{+/+}$ or *Prmt7*$^{-/-}$ mice (n = 20–25) were used. The blood glucose levels were measured after fasting for 16 h with free water. For the glucose and pyruvate tolerance test, mice were fasted for 16 h prior to injection with 1.5g/kg body wt i.p. 20% D-(+)-glucose or 20% pyruvate (Sigma-Aldrich), followed by measurement of blood glucose levels. For the insulin tolerance test, mice were fasted for 5 h and injected with 0.5 IU/kg body wt i.p. insulin (Sigma), followed by measurement of blood glucose levels.

For assessment of metabolic parameters, 5-month-old *Prmt7*$^{+/+}$ and *Prmt7*$^{-/-}$ mice were analyzed with metabolic cages (Panlab Harvard Apparatus). Measurements were performed for 48 h, during which animals had free access to food and water.

For assessment of muscle endurance capacity, *Prmt7*$^{+/+}$ and *Prmt7*$^{-/-}$ mice (n = 10 per group) were tested for the treadmill running and grip strength. For the treadmill running, a Columbus Exer-6M treadmill was used. Prior to exercise, mice were accustomed to the treadmill with a 5-min run at 7 m/min once per day for 5 days. The exercise test was performed on a 10% incline for 8 m/min for 20 min, followed by increase toward 9 m/min until exhaustion. The grip strength of forelimb was measured by a grip strength meter (Bioseb). All grip strength readings (measured in grams) were normalized to body weight. The exercise was assessed every 15 min for a total of 1 h.

Measurement of Metabolite and Lipids

Mice tissues and whole blood were collected at the end of experiments. For assessment of metabolite content, blood serum was separated and plasma insulin was measured by mouse insulin ELISA kits (U-type; Shibayagi Corp.). Triglyceride and nonesterified fatty acid (NEFA) in blood serum were measured by colorimetric assay kits (Wako). For measurement of the hepatic triglyceride content, frozen livers were digested in ethanolic KOH at 55°C

Downloaded from http://diabetesjournals.org/diabetes/article-pdf/65/7/1868/599654/db151500.pdf by guest on 21 April 2025

overnight followed by the extraction of organic layer with 50% ethanol and centrifugation. After addition of 1 μmol/L $MgCl_2$, the collected organic layer was used for analysis of the triglyceride content.

The blood lactate levels were measured with *Prmt7*$^{+/+}$ and *Prmt7*$^{-/-}$ mice (n = 9) before or after a single bout of treadmill running at 10 m/min for 2 h with use of a Lactate Pro2 kit (Arkray).

Cryosections, Histology, and Immunostaining Analysis

Liver was processed through a fixation with 4% paraformaldehyde and sucrose series followed by cryo-embedding and sectioning with 10-μm thickness on a cryostat microtome (Leica). Freshly dissected muscles were snap frozen in optimal cutting temperature and sectioned with 7-μm thickness. NADH dehydrogenase activity was determined by incubation for 30 min with 0.9 mmol/L NADH and 1.5 mmol/L Nitro Blue Tetrazolium (Sigma-Aldrich) in 3.5 mmol/L phosphate buffer (pH 7.4). Succinate dehydrogenase activity was determined by incubation for 1 h with 50 μmol/L sodium succinate and 0.3 mmol/L Nitro Blue Tetrazolium in 114 mmol/L phosphate buffer containing K-EGTA (Sigma-Aldrich). For myosine heavy-chain (Myh) immunostaining, muscle sections were fixed, permeabilized, and processed for incubation with primary antibodies against Myh type I (MyhI), MyhIIa, and MyhIIb (Developmental Studies Hybridoma Bank) and secondary antibodies. Images were captured under Nikon ECLIPS TE-2000U and NIS-Elements F software (Nikon). Myofibers were traced, and their area was measured using ImageJ software. For hematoxylin-eosin staining, cryosections were processed for staining with Mayer hematoxylin-eosin (BBC Biomedical). For periodic acid Schiff staining, liver sections were fixed with Carnoy fixative for 10 min, followed by incubation with 0.5% periodic acid solution (Sigma-Aldrich) for 10 min and counterstaining with Mayer hematoxylin-eosin. For Oil Red O staining, liver sections were fixed and washed with 60% isoprophanol, followed by staining with Oil Red O working solution.

Electron Microscopy and In Vivo Micro–Computed Tomography Imaging

For electron microscopy, tibialis anterior (TA) muscle samples were fixed overnight with 2.5% glutaraldehyde/4% paraformaldehyde solution at 4°C. After incubation for 1 h in 1% OsO_4, the specimens were dehydrated in ethanol series, passed through propylene oxide, and embedded in epoxy resin (Epok). Ultrathin sections (70 nm) were collected on 200 mesh nickel grids and stained for 20 min in 2% uranyl acetate and Reynolds lead citrate. The specimens were observed with a Hitachi HT7700 electron microscope at 100 kV. Electron microscopy was performed by the Research Electron Microscopy Core at Samsung Biomedical Institute.

Microcomputed tomography was performed on a preclinical scanner (Inveon Preclinical CT; Siemens Healthcare) at 200-μm slice thickness, with exposure time of 500 ms, photon energy of 60 keV, and current of 400 μA. The projection images were reconstructed into a three-dimensional image with IRW software. Total abdominal fat volumes including subcutaneous and visceral fat were using Siemens Inveon software.

RNA, Protein Analysis, and Mitochondrial DNA Contents

Quantitative RT-PCR (qRT-PCR) analysis was carried out as previously described (40). Tissues were homogenized by FastPrep^{R}-24 (MP Biomedicals) and extracted with an easy-spin Total RNA Extract kit (iNtRON). All data are normalized to expression of ribosomal gene L32. The primer sequences are shown in Supplementary Table 1.

Western blot analysis was performed as previously described (41,42). Briefly, cells were lysed in cell extraction buffer (10 mmol/L Tris-HCl, pH 8.0; 150 mmol/L NaCl; 1 mmol/L EDTA; and 1% Triton X-100) containing complete protease inhibitor cocktail (Roche), followed by SDS-PAGE and incubation with primary and secondary antibodies. Tissue extracts were prepared by cryo-pulverization with liquid nitrogen and lysed in cell extraction buffer. Primary antibodies used were Prmt7, ATF2, pATF2, Hsp90 (Santa Cruz Biotechnology), CREB, pCREB, p38MAPK, pp38MAPK, pFOXO1, GAPDH, Prmt5, Prmt1 (Cell Signaling Technology), pFoxo1 (Cell Signaling Technology), PGC-1α, Prmt1, SYM10 (Millipore), β-tubulin (Zymed), and hemagglutinin (HA) (AbFrontier).

Immunoprecipitation was performed as previously described (43). Briefly, precleared cell extracts were incubated with primary antibodies overnight at 4°C, followed by incubation with protein G-agarose beads (Roche) for 1 h and washing three times with cell extraction buffer. Precipitates were analyzed by Western blotting.

For mitochondrial DNA contents, total DNA was extracted from TA muscles, hearts, or brown adipose tissue using a DNeasy Blood and Tissue kit (QIAGEN). The amount of mitochondrial DNA was quantified by the ratio of Mtco2 to β-actin by quantitative PCR.

Cell Culture, Constructs, Luciferase Assay, and Chromatin Immunoprecipitation

C2C12 myoblasts (44) and 293T and 10T1/2 cells were cultured as previously described (41). For the generation of stable cell lines, C2C12 cells were transfected with pSuper or pSuper/Prmt7 short hairpin (sh)RNA and selected with 1 μg/mL puromycin followed by pooling the colonies and analyzed. Five different shRNAs against Prmt7, as listed in Supplementary Table 1, were tested and screened for the knockdown effectiveness in P19 embryonal carcinoma cells (Supplementary Fig. 7). Prmt7-shRNA1 and -2 are cloned into pSuper-puro vector based on reproducibility and used interchangeably. Luciferase assays were performed as previously described (45). All experiments were carried out as triplicates and repeated at least three times.

Constructs used in this study are as following: pCMV6-Prmt7 (Origene), CMV–β-galactosidase (33), CRE-Luc (46), and PGC-1α–Luc (Addgene). Chromatin immunoprecipitation (ChIP) assay was carried out as previously described (46). For generation of HA-tagged Prmt7 construct, Prmt7

Downloaded from http://diabetesjournals.org/diabetes/article-pdf/65/7/1868/599654/db151500.pdf by guest on 21 April 2025

was subcloned into a pCDNA3.1-HA vector (Clonetech). Antibodies used for ChIP included rabbit IgG (Millipore), Prmt7 (GeneTex), and ATF2 (Cell Signaling Technology). The primers used to amplify the PGC-1α promoter region between −260 to −54 are listed in Supplementary Table 1. All primer sequences are listed in Supplementary Table 1.

Oxygen Consumption Analysis

Oxygen probe analysis was performed as previously described (47). C2C12/pSuper and C2C12/shPrmt7 were induced to differentiate for 2 days and incubated with a Mito-ID O_2 Probe kit (Enzo) for 4 h followed by washing and analysis by using a fluorescent plate reader in 100 μL DMEM without serum or phenol red. For induction of or inhibition of ATP production, cells were preincubated for 30 min in serum-free DMEM containing 1 μmol/L carbonyl cyanide 4-(trifluoromethoxy)phenylhydrazone (FCCP) (Sigma-Aldrich) or 1 μmol/L antimycin A (Sigma-Aldrich) and covered in mineral oil, followed by analysis using a fluorescent plate reader.

Statistical Analyses

Values are expressed as means ± SD or ± SEM, as indicated in the figure legends. Statistical significance was calculated using paired or unpaired two-tailed Student *t* test. Differences were considered statistically significant at or under values of $P < 0.05$. For comparison between multiple groups, statistical significance was tested by ANOVA test using SPSS (version 12.0; SPSS, Chicago, IL). To control for the influence of body size variation on energy expenditure (EE), we adjusted group comparisons involving this outcome for total body mass using ANCOVA.

RESULTS

Prmt7 Is Highly Expressed in Skeletal Muscles and Its Expression Is Decreased With Age and Obesity

To investigate the in vivo role of Prmt7, we analyzed the level of Prmt7 transcripts in various adult mouse tissues by qRT-PCR. Prmt7 exhibited the highest expression in skeletal muscle, while a modest expression of Prmt7 was detected in heart, brown adipose tissue, kidney, liver, lung, stomach, spleen, white adipose tissue, and small intestine (Fig. 1*A*). It is of note that Prmt7 transcripts were progressively decreased in aging skeletal muscles analyzed with quadriceps muscles from 5-, 10-, or 28-month-old mice (Fig. 1*B*). The age-dependent decrease of Prmt7 correlated well with decreased expression of MyhIIa (oxidative fast-twitch fibers), myoglobin (an oxygen transporter), succinate dehydrogenase subunit b (Sdhb) (a mitochondrial enzyme), and PGC-1α (Fig. 1*B*). In contrast, the expression of MyhI (oxidative slow-twitch fibers) and MyhIIb (glycolytic fast-twitch fibers) was not altered greatly in aging quadriceps. In addition, Prmt7, PGC-1α, and myosin heavy chain (MHC) type IIa (MHCIIa) levels were significantly reduced in gastrocnemius muscles (Gas) from 3-month-old obese mouse models, *ob/ob* and *db/db*, compared with the respective control mice (Fig. 1*C*). These data suggest that Prmt7 expression is decreased in skeletal muscles from aging or obese mouse models, correlated with decreased oxidative muscle metabolism. Hindlimb, Gas, TA, and extensor digitorum longus (EDL) and soleus (Sol) muscles that exhibit distinct metabolic characteristics did not show any specific difference in Prmt7 protein expression (Fig. 1*D* and *E*). The role of Prmt7 in skeletal muscle function was investigated by using 4-month-old $Prmt7^{+/+}$ and $Prmt7^{-/-}$ mice that were obtained from the Sanger Institute and backcrossed onto a C57BL/6J background for at least six generations. $Prmt7^{+/+}$ and $Prmt7^{-/-}$ mice did not differ in body weights or exterior appearance (Fig. 1*F* and *K*, upper panel). The LacZ transgene in $Prmt7^{-/-}$ mice can be readily detected in Gas and TA muscles (Fig. 1*G*). Consistently, Prmt7 proteins were readily detected in Gas muscles of $Prmt7^{+/+}$ mice and were absent in Gas muscles of $Prmt7^{-/-}$ mice (Fig. 1*H*). The organ weights from 4-month-old $Prmt7^{-/-}$ mice did not differ from the wild-type littermates (Fig. 1*I* and Supplementary Table 2). In addition, the weight of $Prmt7^{-/-}$ muscles did not show any significant difference, except for Sol muscles, with a slight but significant decrease (Fig. 1*J* and Supplementary Table 2). Interestingly, skeletal muscles of $Prmt7^{-/-}$ mice appeared pale compared with the wild-type littermates (Fig. 1*K* and *L*). Four-month-old $Prmt7^{-/-}$ muscles did not show any signs of structural abnormalities such as centrally localized nuclei in the histological analysis (Supplementary Fig. 1), suggesting that Prmt7 is dispensable for the gross muscle development. In addition, the histological analysis of white and brown adipose tissue of 4-month-old $Prmt7^{-/-}$ mice showed no obvious difference in the appearance and the cross-sectional area from that of the wild-type mice (Supplementary Fig. 2).

Prmt7-Deficient Muscles Exhibit a Switch Toward Glycolytic Fiber Types

The qRT-PCR analysis of TA muscles from $Prmt7^{+/+}$ and $Prmt7^{-/-}$ mice revealed that Prmt7 deficiency caused a significantly reduced expression of oxidative fiber markers MyhI and –IIa, accompanied by a substantial increase in glycolytic fiber markers MyhIIx and -IIb, compared with wild type (Fig. 2*A*). $Prmt7^{+/+}$ and $Prmt7^{-/-}$ muscles were cryosectioned and immunostained for Myh types. Similarly to the qRT-PCR analysis, $Prmt7^{-/-}$ TA muscles had fewer and smaller MyhIIa-immunopositive fibers, while these contained more and larger MyhIIb-positive fibers, compared with controls (Fig. 2*B* and *C*). In addition, $Prmt7^{-/-}$ Sol muscles showed significantly reduced MyhI-positive fibers in number and size. Similarly, Prmt7 deficiency in EDL muscles resulted in diminished MyhI-positive fibers and increase of MyhIIb fibers in number and size (Supplementary Fig. 3). Skeletal muscles were further assessed by the enzymatic staining for two oxidative enzymes, NADH tetrazolium (NADH-TR) and succinate dehydrogenase (SDH), in TA and EDL muscles. The number of NADH-TR– and SDH-positive fibers and the staining intensities were decreased in $Prmt7^{-/-}$ TA and EDL muscles (Fig. 2*D* and *E*). In addition, $Prmt7^{-/-}$ Gas muscles

Downloaded from http://diabetesjournals.org/diabetes/article-pdf/65/7/1868/599654/db151500.pdf by guest on 21 April 2025

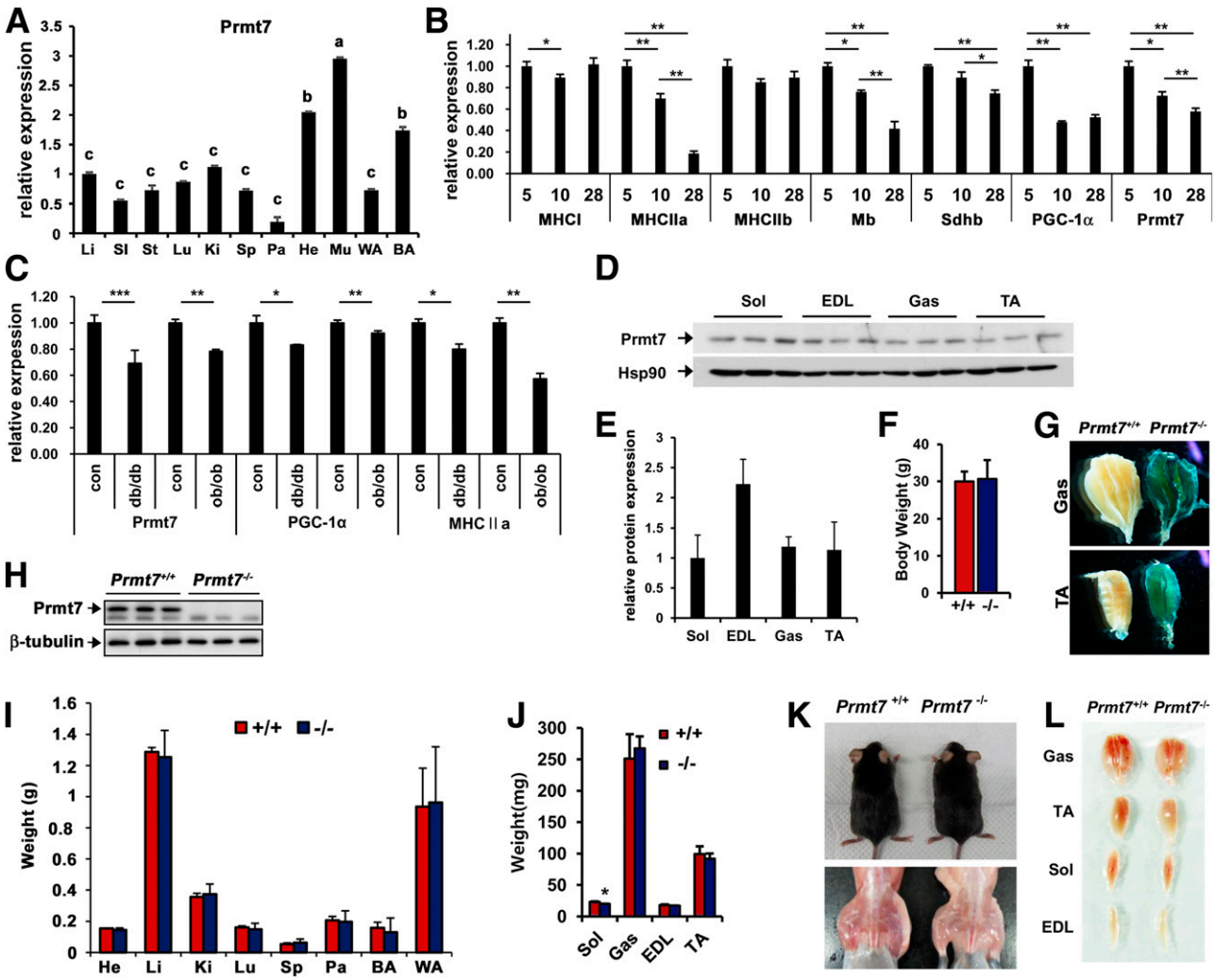

Figure 1—Prmt7 is highly expressed in skeletal muscles, and Prmt7-deficient mice exhibit pale appearance of skeletal muscles. *A*: qRT-PCR analysis of Prmt7 expression in adult tissues (n = 3). Letters indicate statistically distinct groups (ANOVA, Tukey, $P < 0.01$). *B*: qRT-PCR analysis of quadriceps muscles of 5-, 10-, or 28-month-old mice (n = 3 mice per group) for various muscle markers and Prmt7. Data represent means ± SEM. *$P < 0.05$, **$P < 0.01$. *C*: qRT-PCR analysis of Gas muscles of control (con), *db/db*, and *ob/ob* mice (n = 5 per group) for Prmt7, PGC-1α, and MHCIIa. Data represent means ± SEM. *$P < 0.05$, **$P < 0.01$, ***$P < 0.001$. *D*: Prmt7 protein expression in low hindlimb muscle types from adult mice (n = 3). *E*: The quantification of normalized Prmt7 signal intensity relative to control Hsp90 shown in *D*. Data represent means ± SD. *F*: Body weights of 4-month-old $Prmt7^{+/+}$ and $Prmt7^{-/-}$ mice (n = 5). Data represent means ± SD. *G*: The LacZ staining for the transgene β-galactosidase in $Prmt7^{-/-}$ Gas and TA muscles. *H*: Western blot analysis for Prmt7 expression in Gas muscles from 4-month-old $Prmt7^{+/+}$ and $Prmt7^{-/-}$ mice (n = 3). *I*: Organ weights of 4-month-old $Prmt7^{+/+}$ and $Prmt7^{-/-}$ mice. *J*: Weights of 4 muscle types from $Prmt7^{+/+}$ and $Prmt7^{-/-}$ mice (n = 5 per group). Data represent means ± SD. *$P <$ 0.05. *K*: Pictures of 4-month-old $Prmt7^{+/+}$ and $Prmt7^{-/-}$ male mice. *L*: Photograph of isolated muscle types from the low hindlimbs from 4-month-old $Prmt7^{+/+}$ and $Prmt7^{-/-}$ mice. BA, brown adipose tissue; He, heart; Ki, kidney; Li, liver; Lu, lung; Pa, pancreas; Sl, small intestine; Sp, spleen; St, stomach; Mu, skeletal muscle; WA, white adipose tissue.

had more weakly stained myofibers for both NADH-TR and SDH staining; however, $Prmt7^{-/-}$ Sol muscles did not exhibit any significant difference from the wild-type muscles (Supplementary Fig. 4*A* and *B*). Taken together, Prmt7-deficient muscles exhibit the oxidative to glycolytic fiber-type switch.

Prmt7 Deficiency Reduced Oxidative Muscle Metabolism and Impaired Endurance Muscle Function

The expression of genes involved in the regulation of various muscle functions, Mef2c, Fndc5, myoglobin (muscle), Mcad, Mtco1, Sdhb, Cox7a1, Ucp2 (mitochondria), Fabp3, VLDLR, CideA (lipid metabolism and mitochondria), Vegfα, Vegfβ (angiogenesis) and Glut4, and PEPCK (glucose metabolism), was examined by qRT-PCR analysis (Fig. 3*A* and *B*). Myoglobin expression was reduced roughly to 60% of the control level in both $Prmt7^{-/-}$ TA and EDL muscles, and this likely contributed to the pale appearance of $Prmt7^{-/-}$ muscles seen in Fig. 1*L*. Among mitochondrial genes, Mtco1, Sdhb, and Ucp2 and angiogenic factors Vegfα and Vegfβ, which are implicated in oxidative muscle functions, were expressed significantly less in $Prmt7^{-/-}$

Downloaded from http://diabetesjournals.org/diabetes/article-pdf/65/7/1868/599654/db151500.pdf by guest on 21 April 2025

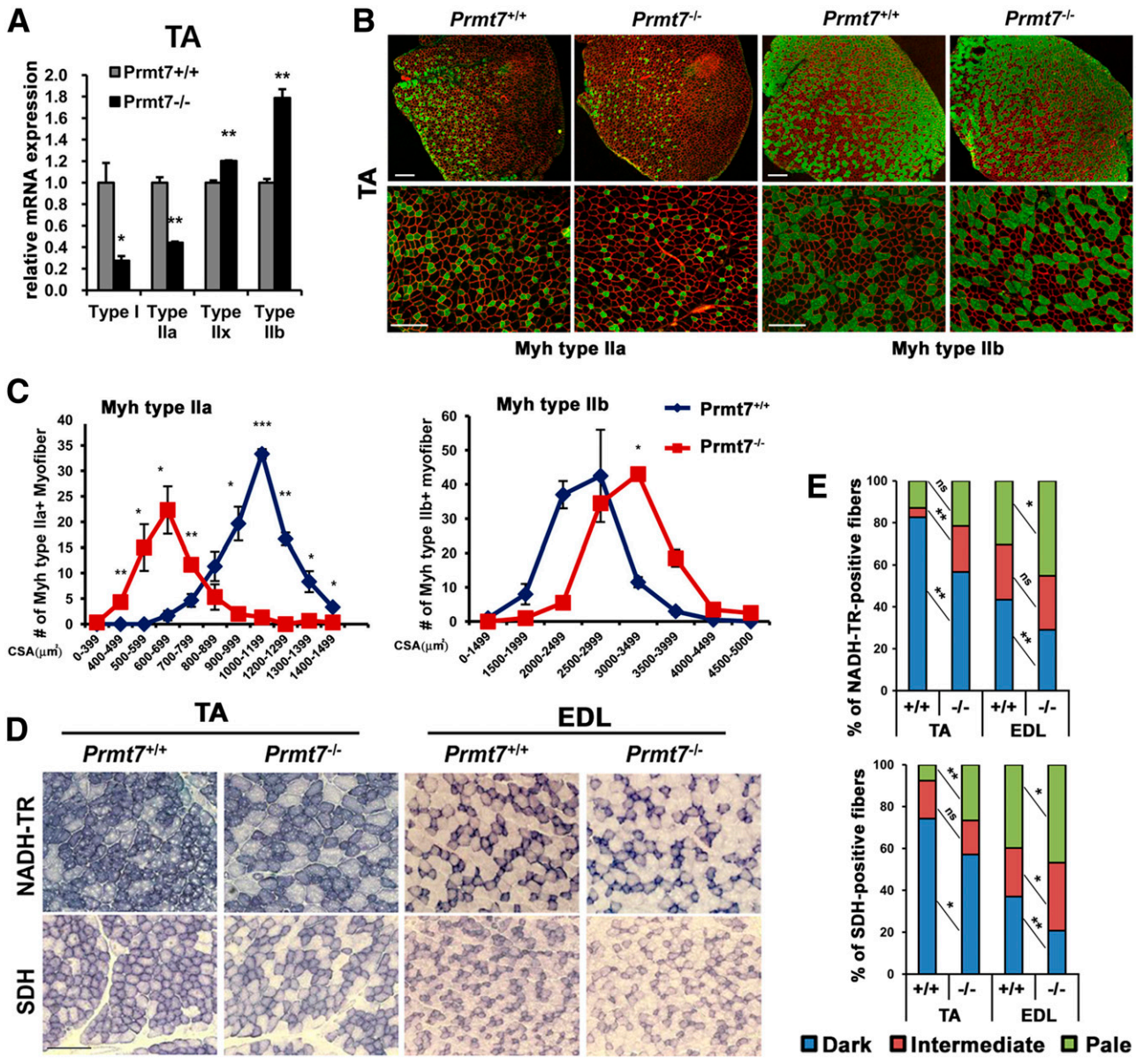

Figure 2—Prmt7 deficiency causes a fiber-type switch toward glycolytic. *A*: qRT-PCR of TA muscles from 4-month-old *Prmt7*$^{+/+}$ and *Prmt7*$^{-/-}$ mice for different Myh types (n = 5 per group). Data represent means ± SEM. *P < 0.05, **P < 0.01. *B*: Immunostaining of 4-month-old *Prmt7*$^{+/+}$ and *Prmt7*$^{-/-}$ TA muscles for MyhIIa and MyhIIb. Scale bars, 100 μm. *C*: Quantification of the cross-sectional area (CSA) of MyhIIa- or MyhIIb-positive myofibers in TA muscles (n = 3). Data represent means ± SEM. *P < 0.05, **P < 0.01, ***P < 0.001. *D*: Histochemical staining of NADH-TR and SDH enzymatic activity in 4-month-old TA and EDL muscles (n = 5 per group). Scale bar, 100 μm. *E*: Quantification of stained myofibers by 3 different staining grades (n = 5). Data represent means ± SEM. ***P < 0.001, **P < 0.01, *P < 0.05. ns, not significant.

muscles. In addition, the expression of PEPCK was also reduced in *Prmt7*$^{-/-}$ muscles, compared with wild type, while a glucose transporter, Glut4, was not greatly changed. Among lipid binding and metabolism regulators, VLDLR was increased in both muscle types, while Fabp3 and CideA expression was decreased. Since many of these genes are targets of PGC-1α, a key regulator of the oxidative metabolism and mitochondrial function (9,14), we assessed the expression of PGC-1α and related genes (PGC-1β, PPARα, and PPARγ) (Fig. 3*C* and *D*). The expression of PGC-1α, PPARα, and PPARγ was greatly decreased in both EDL and TA muscles from *Prmt7*$^{-/-}$ mice, while PGC-1β was reduced only in TA but not in EDL muscles compared with wild types. In the transmission electron microscopy analysis, *Prmt7*$^{-/-}$ TA muscles displayed reduced mitochondrial content compared with wild type (Fig. 3*E* and *F*). Consistently, the relative mitochondrial DNA content was decreased in *Prmt7*$^{-/-}$ TA muscles compared with the *Prmt7*$^{+/+}$ muscles (Fig. 3*G*). In contrast, *Prmt7*$^{-/-}$ hearts and brown adipose tissues exhibited no difference in mitochondrial DNA content compared with the *Prmt7*$^{+/+}$ tissues (Supplementary Fig. 5*A* and *B*).

Downloaded from http://diabetesjournals.org/diabetes/article-pdf/65/7/1868/599654/db151500.pdf by guest on 21 April 2025

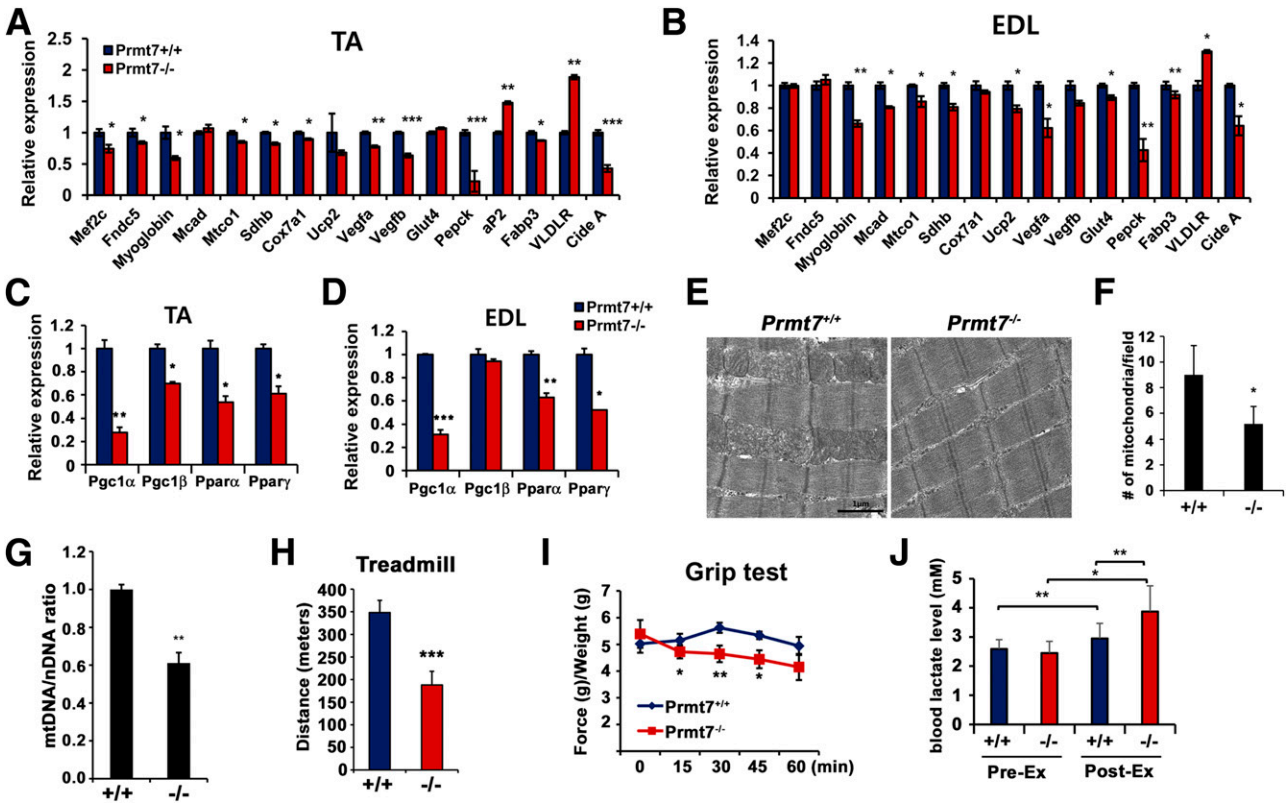

Figure 3—Prmt7 deficiency results in reduced endurance exercise capacities. *A* and *B*: qRT-PCR analysis of gene expression in TA (*A*) and EDL (*B*) muscles of 4-month-old mice (n = 5–6). Data represent means ± SEM. *P < 0.05, **P < 0.01, ***P < 0.001. *C* and *D*: qRT-PCR analysis for PGC-1 cofactors and PPARs in TA (*C*) and EDL (*D*) muscles (n = 5 mice). Data represent means ± SEM. *P < 0.05, **P < 0.01, ***P < 0.001. *E*: Transmission electron micrographs of TA muscles isolated from 4-month-old $Prmt7^{+/+}$ and $Prmt7^{-/-}$ mice. Scale bar, 1 μm. *F*: Mean numbers of mitochondria per transmission electron micrograph field shown in *E*. Values were calculated from total 9 fields of 3 different samples. Data represent means ± SD. *P < 0.05. *G*: The relative mitochondrial DNA (mtDNA)–to–nuclear DNA (nDNA) ratio. The mitochondrial content was estimated using the relative expression ratio of mitochondrial DNA (Mtco2) to nuclear DNA (β-actin). The values from $Prmt7^{+/+}$ mice were set to 1. Values are means ± SEM (n = 3 per group). *H*: The endurance activity on the treadmill running is depicted as distance (n = 10). *I*: Grip strength is depicted by force per weight that animals in each group pulled (n = 10). *J*: Blood lactate levels in serum from mice prior to or after the treadmill running for 2 h (n = 9). Data represent means ± SD. *P < 0.05, **P < 0.01. Pre-Ex, pre-exercise; Post-Ex, after a single bout of treadmill exercise.

The functional consequence of this switch was assessed by treadmill running and the repeated grip tests at every 15 min for a 1-h period. On the treadmill, $Prmt7^{-/-}$ mice ran a significantly shorter distance compared with the wildtype littermates (Fig. 3*H*). However, these mice had stronger grip strengths at the initial time point, which then declined significantly during the repeated training time points, whereas wild-type mice sustained their muscle strength (Fig. 3*I*). In addition, the basal lactate level in pre-exercise $Prmt7^{+/+}$ and $Prmt7^{-/-}$ mice showed no significant difference. After a single bout of treadmill exercise, it increased in both mice groups, but Prmt7-deificent mice displayed significantly higher lactate levels compared with the wild-type mice (Fig. 3*J*). Taken together, these results indicate that Prmt7 deficiency results in reduced oxidative muscle metabolism and impaired endurance muscle capacity.

Mice Lacking Prmt7 Exhibit Decreased Energy Expenditure

We then have assessed the whole-body metabolic rates with 5-month-old $Prmt7^{+/+}$ and $Prmt7^{-/-}$ mice. $Prmt7^{+/+}$ and $Prmt7^{-/-}$ mice did not exhibit any significant difference in body weights, food and water intake, or spontaneous locomotive or rearing activity relative to $Prmt7^{+/+}$ mice (Fig. 4*A*–*E*). $Prmt7^{-/-}$ mice exhibited a significant decrease in total EE, respiratory quotient, VO_2, and VCO_2 compared with wildtype mice (Fig. 4*F*–*J*). These results suggest that Prmt7 deficiency causes decreased EE.

Mice Lacking Prmt7 Develop Obesity With Excessive Body Fat Accumulation at Middle Age

The alteration of metabolic characteristics and the decreased PGC-1α level in skeletal muscle are associated with various metabolic pathologies such as obesity (17,21). The shift from oxidative to glycolytic fibers and the decreased expression of PGC-1α in Prmt7-deficient mice predicted a metabolic phenotype such as obesity. Four-month-old $Prmt7^{+/+}$ and $Prmt7^{-/-}$ mice showed no difference in body weights (Fig. 1*F*); however, thereafter $Prmt7^{-/-}$ mice gained progressively more weight relative to wild-type littermates. At ~10–12 months of age, $Prmt7^{-/-}$ mice became obviously fatter than littermates, and this

Downloaded from http://diabetesjournals.org/diabetes/article-pdf/65/7/1868/599654/db151500.pdf by guest on 21 April 2025

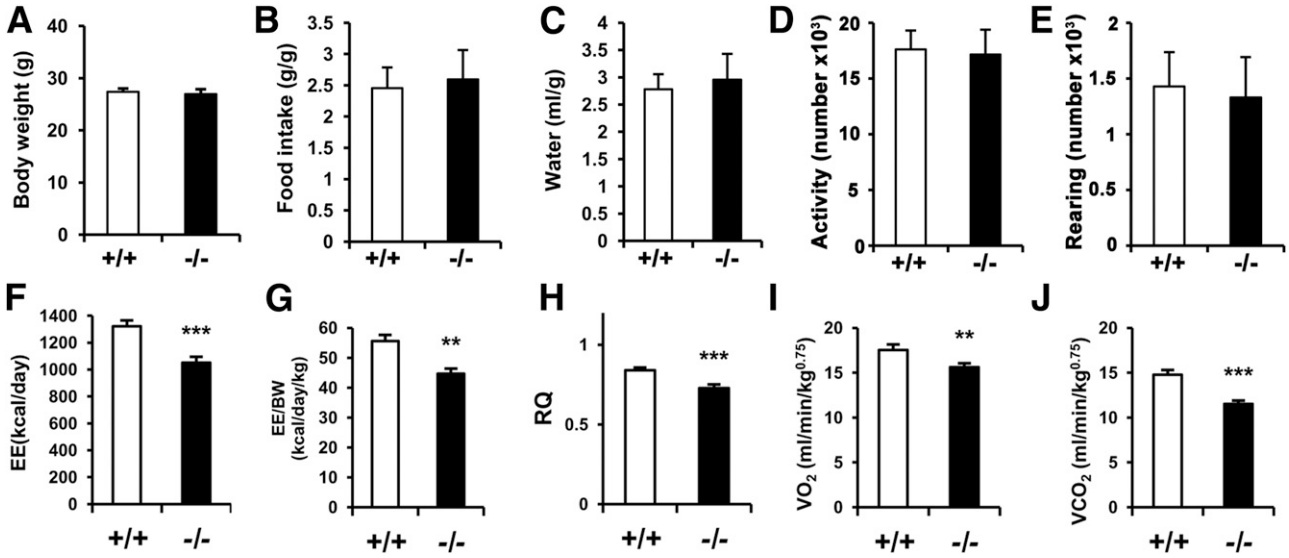

Figure 4—*Prmt7*$^{-/-}$ mice exhibit decreased EE. Normal chow-fed, 5-month-old *Prmt7*$^{+/+}$ and *Prmt7*$^{-/-}$ mice were analyzed with metabolic cages (n = 6). Data in *A*–*J* represent means ± SEM. *P < 0.05, **P < 0.01, ***P < 0.001. *A*: Body weights. *B*: Food intake. *C*: Drinking water. *D*: Locomotive activities. *E*: Rearing activities. *F*: Absolute values of EE. *G*: The adjusted means of EE in the two groups analyzed by ANCOVA with body weight (BW). *H*: respiratory quotient (RQ). *I* and *J*: VO_2 and VCO_2.

obese phenotype was observed in both female and male mice (Fig. 5*A* and *B*). The excessive body fat accumulation was observed in 13-month-old *Prmt7*$^{-/-}$ female mice compared with the wild-type littermates (Fig. 5*A*). This was further confirmed by micro–computed tomography scan analyses of 12-month-old *Prmt7*$^{+/+}$ and *Prmt7*$^{-/-}$ male mice that showed roughly 1.5-fold more body fat accumulation compared with wild-type littermates (Fig. 5*B* and *C*). Livers from three 12-month-old *Prmt7*$^{+/+}$ and *Prmt7*$^{-/-}$ littermates were assessed, and two *Prmt7*$^{-/-}$ mice exhibited enlarged livers with excessive lipid accumulation analyzed by Oil Red O staining compared with that of a wild-type littermate (Fig. 5*D*). The histological analysis of white adipose tissues and brown adipose tissues from 8-month-old *Prmt7*$^{+/+}$ and *Prmt7*$^{-/-}$ mice revealed that Prmt7 deficiency resulted in enlarged white adipocytes and enhanced lipid droplet accumulation in brown adipocytes (Supplementary Fig. 6). For assessment of the metabolic consequence in *Prmt7*$^{-/-}$ mice, the glucose, insulin, and pyruvate tolerance tests were carried out with 12-month-old *Prmt7*$^{+/+}$ and *Prmt7*$^{-/-}$ mice. *Prmt7*$^{-/-}$ mice displayed impaired glucose and insulin sensitivity (Fig. 5*E* and *F*), without alterations in pyruvate tolerance, suggesting that the hepatic gluconeogenesis is normal (Fig. 5*G*). In addition, *Prmt7*$^{-/-}$ mice displayed increased fasting blood glucose levels relative to *Prmt7*$^{+/+}$ littermates (Fig. 5*H*) without any significant difference in the food intake (Fig. 5*I*) or in circulating leptin or fasting insulin level (Fig. 5*J* and *K*). However, the plasma NEFA, plasma, and hepatic triglyceride content increased significantly in *Prmt7*$^{-/-}$ mice relative to the wild-type control (Fig. 5*L*–*N*). Taken together, these data suggest that Prmt7 deficiency in mice causes age-dependent obesity and hyperglycemia without altered energy intake, leptin, or insulin levels.

Prmt7 Depletion Reduces PGC-1α Expression and the PGC-1α Reporter Activities in Myoblasts

The phenotypic characteristics of PGC-1α (21) and Prmt7-deficient mice are similar, and PGC-1α was decreased considerably in Prmt7-deficient muscles. Thus, we examined whether Prmt7 regulates oxidative muscle metabolism via regulation of PGC-1α expression. C2C12 myoblasts were used to assess the effect of Prmt7 depletion. We tested five Prmt7 shRNAs (shPrmt7) in p19 embryonal carcinoma and all five showed efficient knockdown effects (Supplementary Fig. 7), and shPrmt7-1 or -2 were subcloned into pSuper-puro vector. C2C12 cells were transfected with the control pSuper or shPrmt7 vector, and the transfectants were selected with puromycin. C2C12/pSuper or C2C12/shPrmt7 were induced to differentiate by transferring cells into 2% horse serum containing medium for a total of 2 days, and we analyzed the expression of Prmt7, MHC, and myogenin protein (Fig. 6*A*) and the mRNA expression of PGC-1α, Mef2c, myoglobin, Mtco1, and Sdhb (Fig. 6*B* and *E*). C2C12/shPrmt7 cells exhibited decreased Prmt7 levels relative to the control C2C12/pSuper cells, and the knockdown effect was strongest at day 1 (D1), while it was weaker at D2. C2C12/shPrmt7 cells showed reduced levels of myogenin and MHC expression at D2 compared with the control cells, suggesting a role of Prmt7 for myoblast differentiation. PGC-1α, Mef2c, and myoglobin transcription was markedly increased in differentiating control C2C12/pSuper cells (Fig. 6*B*–*D*). Consistent with the results obtained from Prmt7-deficient muscle analysis,

Downloaded from http://diabetesjournals.org/diabetes/article-pdf/65/7/1868/599654/db151500.pdf by guest on 21 April 2025

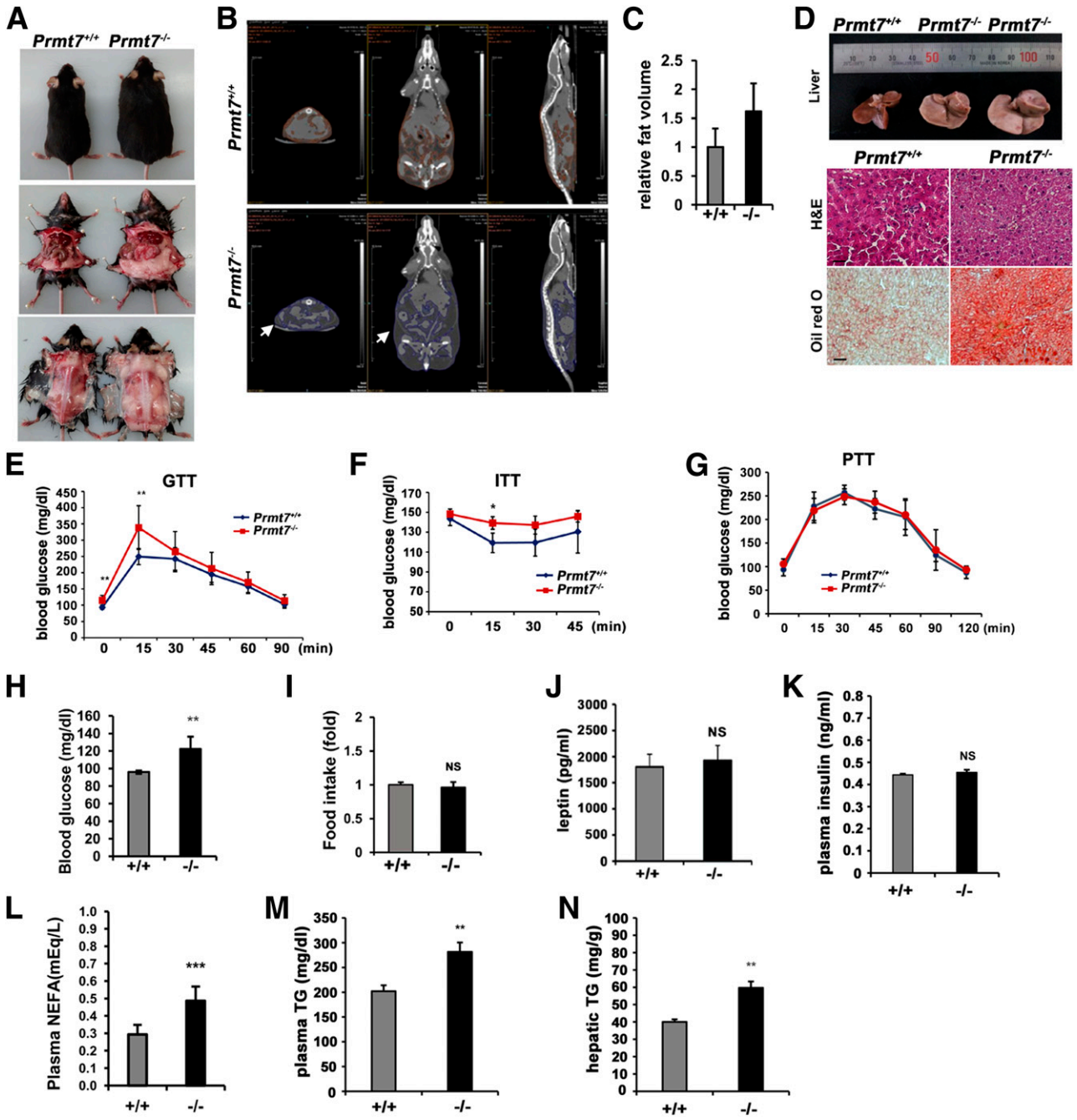

Figure 5—Prmt7-deficient mice become obese in middle age. *A*: Photographs of 13-month-old female *Prmt7*$^{+/+}$ and *Prmt7*$^{-/-}$ littermates. *B*: Micro–computed tomography scan of 12-month-old male *Prmt7*$^{+/+}$ and *Prmt7*$^{-/-}$ mice. Note the excessive body fat accumulation in *Prmt7*$^{-/-}$ mice, marked with arrows. *C*: Quantification of the body fat volume of 12-month-old mice (n = 5). *D*: Photographs of liver from 12-month-old littermates with indicated genotypes (upper panel). Histology of liver cryosections stained with hematoxylin-eosin (H&E) or Oil Red O. Scale bars, 10 μm. *E*–*G*: Glucose (GTT), insulin (ITT), and pyruvate (PTT) tolerance tests with 12-month-old *Prmt7*$^{+/+}$ and *Prmt7*$^{-/-}$ mice fed with normal chow (n = 8). *P < 0.05, **P < 0.01. *H*: Fasting glucose levels of 12-month-old mice (n = 8). **P < 0.01. *I*: Relative food intake per day of 12-month-old *Prmt7*$^{+/+}$ and *Prmt7*$^{-/-}$ mice (n = 8). *J*–*M*: Blood leptin levels (*J*), insulin levels (*K*), NEFA levels (*L*), and triglyceride (Tg) levels (*M*) of 12-month-old mice (n = 7). *N*: Hepatic triglyceride levels of 12-month-old mice (n = 7). Data represent means ± SD. *P < 0.05, **P < 0.01.

Prmt7 knockdown C2C12 cells exhibited significantly reduced expression of PGC-1α at D1, which was further decreased at D2 (Fig. 6*B*). Furthermore, the expression of Mef2c, myoglobin (Fig. 6*C* and *D*), Mtco1, and Sdhb (Fig. 6*E*) was significantly reduced in these cells at D2 relative to control shRNA-expressing cells. We then examined whether these decreased levels of PGC-1α, Mtco1, and Sdhb have any effect on basal respiration (Fig. 6*F*) using control and Prmt7 knockdown C2C12 cells at D2. Prmt7 knockdown led to reduced oxygen consumption under basal

Downloaded from http://diabetesjournals.org/diabetes/article-pdf/65/7/1868/599654/db151500.pdf by guest on 21 April 2025

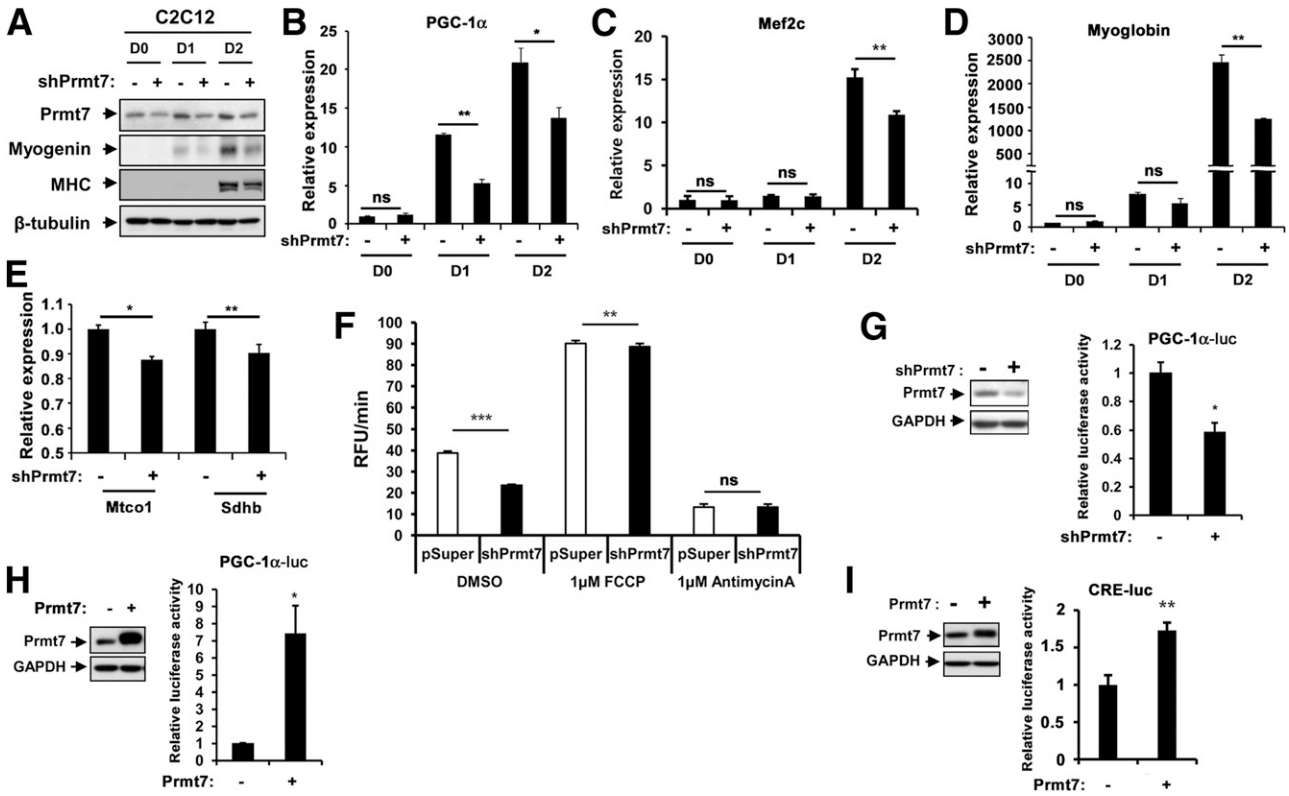

Figure 6— Prmt7 depletion reduces PGC-1α expression and PGC-1α promoter activities in C2C12 myoblasts. *A*: The control Western blots for Prmt7 expression in C2C12 cells expressing control pSuper or shPrmt7. *B–D*: qRT-PCR analysis of control or shPrmt7-expressing C2C12 cells at D0, D1, or D2 for PGC-1α, Mef2c, or myoglobin expression. Values are means of triplicates ± SD. **P* < 0.05, ***P* < 0.01. *E*: qRT-PCR analysis of control or shPrmt7-expressing C2C12 cells at D2 for the mitochondrial genes, Mtco1 and Sdhb. Values are means of triplicates ± SD. **P* < 0.05. *F*: Oxygen consumption in control pSuper or shPrmt7-transfected C2C12 cells at D2. For modulation of the ATP production, cells were treated with 1 μmol/L FCCP or 1 μmol/L antimycin A. Values are means of triplicates ± SEM. ***P* < 0.01, ****P* < 0.001. *G*: The control Western blots for Prmt7 expression in control or shPrmt7-expressing C2C12 cells (left panel). The relative PGC-1α luciferase activity in C2C12 cells transfected with control or shPrmt7 (right panel). *H*: The control Western blots for Prmt7 expression in control or Prmt7-overexpressing C2C12 cells (left panel). The relative PGC-1α luciferase activity in C2C12 cells transfected with control or Prmt7 (right panel). Values are means of triplicates ± SD. **P* < 0.05, ***P* < 0.01. This experiment was performed as triplicates and repeated at least 3 times with similar results. *I*: The control Western blots for Prmt7 expression in control or Prmt7-overexpressing C2C12 cells (left panel). The relative CRE-responsive luciferase activity in C2C12 cells transfected with pcDNA or Prmt7 (right panel). Values are means of triplicates ± SD. ***P* < 0.01. The reporter assays in this figure were performed as triplicates and repeated at least 3 times with similar results. ns, not significant; RFU, relative fluorescence unit.

DMSO-treated conditions. However, the maximal mitochondrial oxidative capacity assessed by FCCP-mediated uncoupling did not differ between two groups of cells, suggesting that the mitochondrial functions are normal.

We tested whether Prmt7 regulates PGC-1α transcription by using a luciferase reporter construct containing the PGC-1α promoter region ranging from 43 to −870 (PGC-1α–Luc). Prmt7 depletion reduced luciferase activities roughly to 60% of that in the control shRNA cells (Fig. 6*G*), while Prmt7 overexpression markedly enhanced the PGC-1α–Luc activities—approximately sevenfold above control levels (Fig. 6*H*). This promoter region of PGC-1α-Luc contains a CRE sequence and a binding site for transcription factors CREB and ATF2, which can be activated through phosphorylation by protein kinases Ca2+/calmodulin-dependent protein kinase and p38, respectively. Consistently, Prmt7 overexpression en-hanced a reporter activity controlled by CRE (CRE-Luc) in C2C12 cells (Fig. 6*I*). These data suggest that Prmt7 regulates PGC-1α expression in C2C12 myoblasts during differentiation.

Prmt7 Depletion Reduces p38 Activation, While Prmt7 Overexpression Enhances It

To further determine the molecular mechanism of PGC-1α regulation by Prmt7, we have examined the activation status of CREB, FOXO1, ATF2, and p38 by immunoblotting with antibodies recognizing active phosphorylated forms of these proteins in control or Prmt7 shRNA-expressing C2C12 cells at D1. The level of an active phosphorylated form of CREB (pCREB) and Foxo1 (pFOXO1) or total CREB was unaltered by Prmt7 depletion in C2C12 cells, while the level of ATF2 phosphorylation (pATF2) was decreased without changes in total ATF2 levels (Fig. 7*A* and *B*). Furthermore, the level of an active phosphorylated form of p38 (pp38) was diminished without changes in total p38 levels (Fig. 7*A* and *B*). These data predicted

Downloaded from http://diabetesjournals.org/diabetes/article-pdf/65/7/1868/599654/db151500.pdf by guest on 21 April 2025

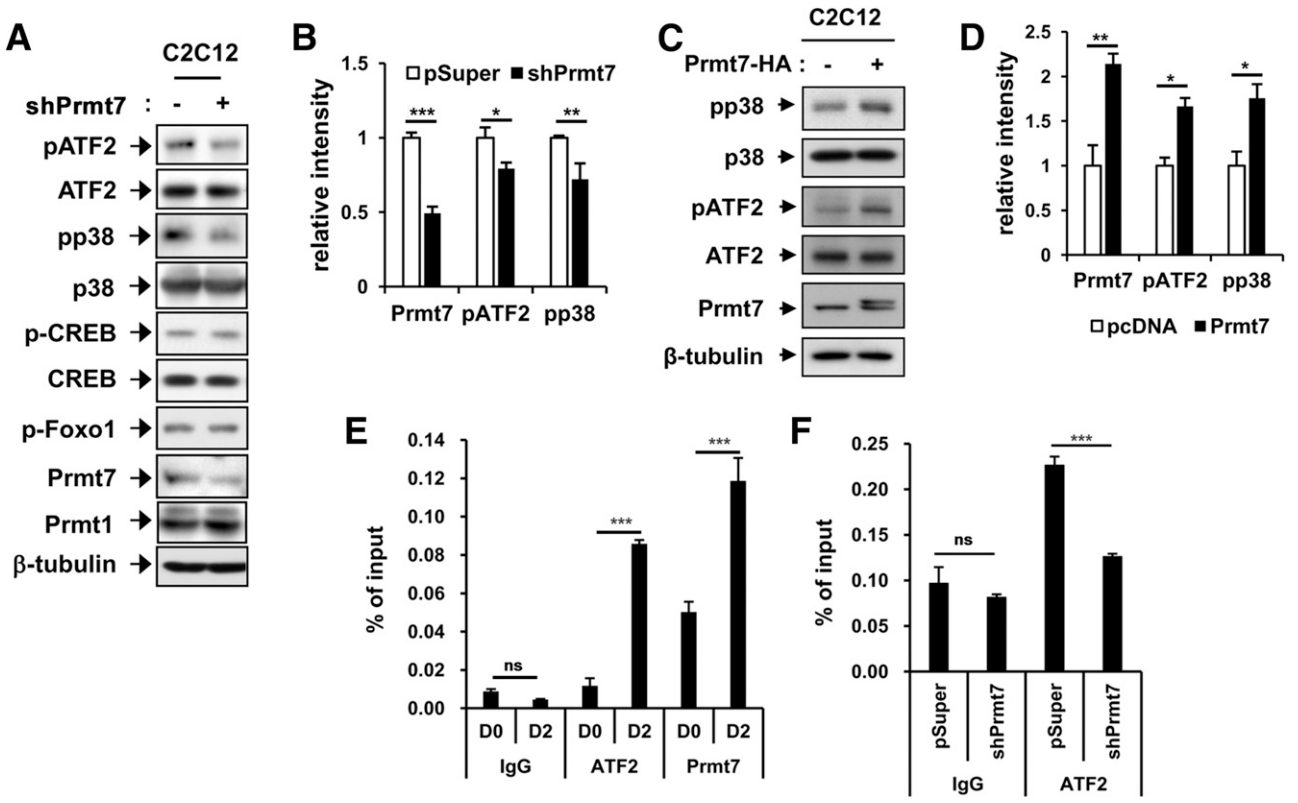

Figure 7—Prmt7 depletion reduces p38 activation, while Prmt7 overexpression enhances it. *A*: Immunoblot analysis of C2C12/pSuper or C2C12/shPrmt7 cells at D1 for expression of various regulators of PGC-1α expression. *B*: Quantification of the relative protein levels of Prmt7, pATF2, and pp38 from three different immunoblots (similar to *A*). The intensity of Prmt7, pATF2, and pp38 was normalized to β-tubulin, total ATF2, and total p38, respectively. The value of the control pSuper cells was set to 1.0. $N = 3$, ±SD. $^{*}P < 0.05$, $^{**}P < 0.01$, $^{***}P < 0.001$. *C*: Immunoblot analysis of control C2C12/pcDNA3.1 or C2C12/Prmt7 cells at D1 for expression of various regulators of PGC-1α expression. *D*: Quantification of the relative protein levels of Prmt7, pATF2, and pp38 from three different immunoblots (similar to *C*). The intensity of Prmt7, pATF2, and pp38 was normalized to β-tubulin, total ATF2, and total p38, respectively, and the determinant of the control cells was set to 1.0. $N = 3$, ±SD. $^{*}P < 0.05$, $^{**}P < 0.01$, $^{***}P < 0.001$. *E*: ChIP assay for the binding of ATF2 and Prmt7 to the CRE sites of the PGC-1α promoter region in C2C12 cells at D0 or D2. Values are expressed as a percentile of input and means of triplicates ± SD. $^{***}P < 0.001$. *F*: The relative enrichment of ATF2 at CRE boxes of the PGC-1α promoter region in C2C12/pSuper or C2C12/shPrmt7 cells at D2. Values are expressed as a percentile of input and means of triplicates ± SD. $^{***}P < 0.001$. ns, not significant.

that Prmt7 may regulate PGC-1α expression through a p38-ATF2 pathway. Previously, it has been shown that Prmt1 regulates p38 activation via interaction and methylation in regulation of megakaryocyte and erythroid differentiation (48). The level of Prmt1 protein was slightly elevated in Prmt7-depleted C2C12 cells (Fig. 7*A*), suggesting that the decreased p38 activation might be specific to Prmt7 depletion. Furthermore, Prmt7 overexpressing C2C12 cells at D1 exhibited elevated levels of pATF2 and pp38 compared with the control C2C12/pcDNA3.1 cells (Fig. 7*C* and *D*).

To determine whether ATF2 and Prmt7 are recruited to CRE sites of the PGC-1α promoter region in C2C12 cells during differentiation, we carried out ChIP analyses. In agreement with previous reports (23,24), the enrichment of ATF2 was greatly enhanced at CRE sites in C2C12 cells at D2 compared with undifferentiated cells (D0). Prmt7 recruitment at CRE sites was also enhanced in differentiating C2C12 cells (Fig. 7*E*). However, the ATF2 enrichment to CRE sites of the PGC-1α promoter region was reduced in C2C12/shPrmt7 cells at D2 (Fig. 7*F*). These results suggest that Prmt7 regulates PGC-1α expression through p38 and ATF2.

Methylation Inhibition Abolishes p38 Activation Induced by Prmt7

We then tested the possibility of an interaction of Prmt7 with p38, thereby activating p38 in myoblast differentiation. p38 was immunoprecipitated specifically with a Prmt7 antibody in C2C12 cells (Fig. 8*A*). To corroborate this notion, we evaluated the potential role of Prmt7 in p38 activation. Prmt7 was coimmunoprecipitated with a p38 antibody, and the level of pp38 concomitantly increased in Prmt7-overexpressing 293T cells compared with the control cells (Fig. 8*B*). Previous reports have shown that p38 can be dimethylated at arginine residues, whereby its activity is modulated (49). Thus, we tested whether p38 can be symmetrically methylated by Prmt7 by using an antibody recognizing symmetric dimethylation of arginine (Sym10). Prmt7-overexpressing 293T cells

Downloaded from http://diabetesjournals.org/diabetes/article-pdf/65/7/1868/599654/db151500.pdf by guest on 21 April 2025

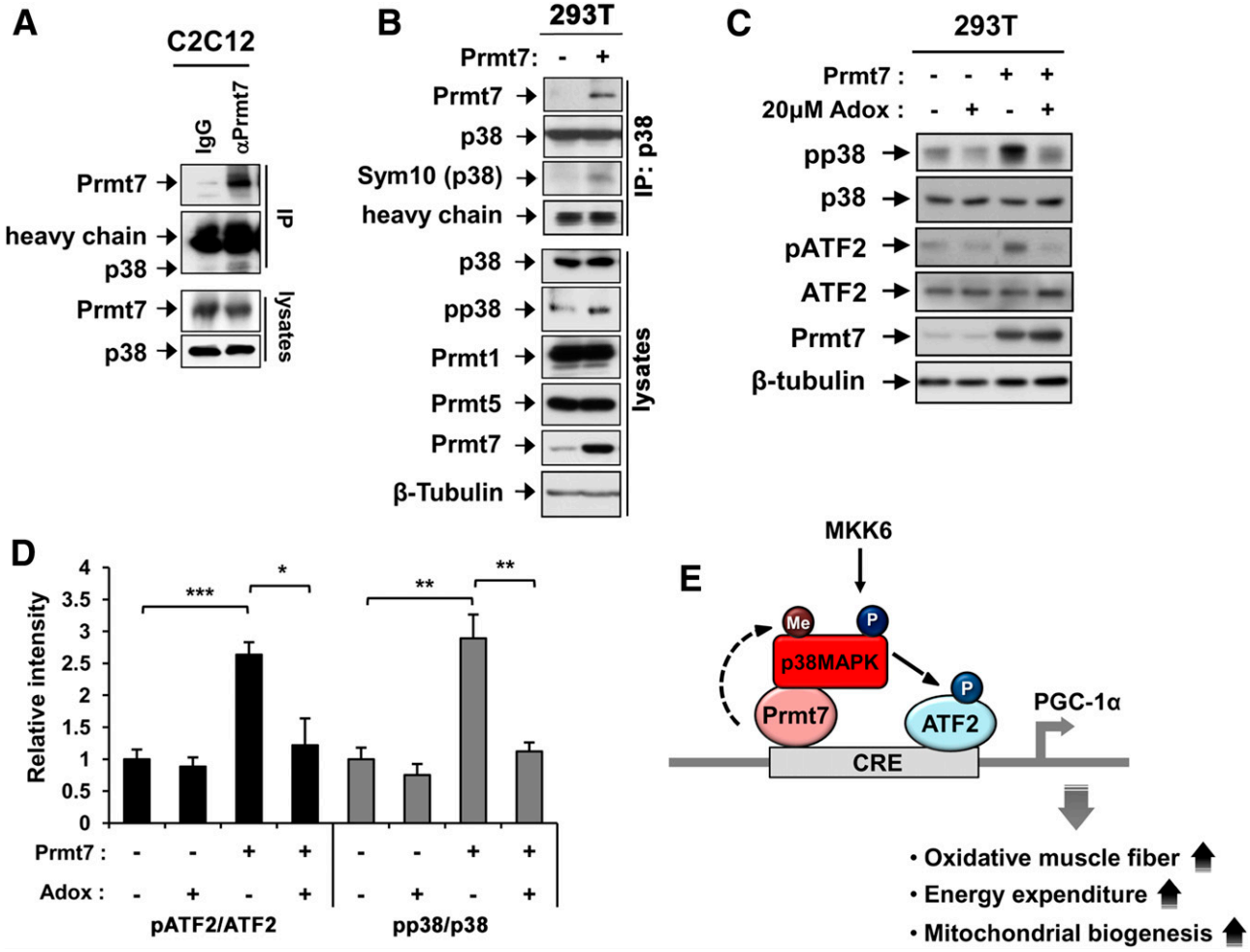

Figure 8—Inhibition of methylation abolishes p38 activation induced by Prmt7. *A*: Coimmunoprecipitation of C2C12 cells at D1 with antibodies to control IgG or Prmt7. *B*: Coimmunoprecipitation of control or Prmt7-overexpressing 293T cells with p38 antibodies and immunoblot analysis with indicated antibodies. This experiment was performed as triplicates and repeated at least 3 times with similar results. *C*: Immunoblot analysis of control pcDNA3.1 or Prmt7-overexpressing 293T cells treated with vehicle or 20 μmol/L Adox for 12 h. *D*: Quantification of the relative protein levels of pATF2 and pp38 from three different immunoblots (similar to *C*). The intensity of pATF2 and pp38 was normalized to total ATF2 and total p38, respectively, and the determinant of the control cells treated with vehicle DMSO was set to 1.0. $N = 3$, ±SD. $^{*}P < 0.05$, $^{**}P < 0.01$, $^{***}P < 0.001$. *E*: Model of Prmt7 regulation of PGC-1α expression. Prmt7 regulates p38MAPK activation, likely through arginine methylation, which in turn activates ATF2 by phosphorylation and enhances its recruitment to the CRE element of the PGC-1α promoter region, leading to induction of PGC-1α expression. IP, immunoprecipitation; MKK6, MAPK kinase 6.

showed enhanced Sym10-postive p38 proteins, and this enhancement occurred without alterations in the expression of Prmt1 or Prmt5 (Fig. 8*B*). For assessment of whether the methyltransferase activity of Prmt7 is required for p38 activation, control or Prmt7-overexpressing 293T cells were treated with the vehicle DMSO or a methyltransferase inhibitor, adenosine dialdehyde (Adox), at a concentration of 20 μmol/L for 12 h and subjected to immunoblotting (Fig. 8*C* and *D*). The control 293T cells treated with Adox exhibited a slight decline of pp38 and pATF2, while the robust increase of pp38 and pATF2 levels in Prmt7-overexpressing cells was abrogated by Adox treatment. These data suggest that the methyltransferase activity is required for p38 activation by Prmt7.

Previously, it has been shown that Prmt1 methylates and activates PGC-1α, thereby inducing its target genes, like ERRα and cytochrome c (35). To examine whether, like Prmt1, Prmt7 might activate PGC-1α through interaction and methylation, we performed coimmunoprecipitation analysis between PGC-1α and Prmt7 in 293T cells (Supplementary Fig. 8*A–C*). Prmt7 and PGC-1α failed to form complexes, while Prmt1 interacted with PGC-1α as shown in a previous study (35). In summary, Prmt7 regulates PGC-1α expression through activation of p38/ATF2, thereby enhancing mitochondrial biogenesis and oxidative muscle metabolism (Fig. 8*E*). Prmt7 deficiency causes a shift toward glycolytic muscle metabolism, blunting maximum muscle endurance capacity. These alterations in skeletal muscle cause impaired EE, resulting in

Downloaded from http://diabetesjournals.org/diabetes/article-pdf/65/7/1868/599654/db151500.pdf by guest on 21 April 2025

the excessive energy storage associated with exacerbation of the age-related obesity.

DISCUSSION

In this study, we demonstrate that Prmt7 is a critical regulator for the oxidative metabolism and the endurance function of skeletal muscle. Mice lacking Prmt7 develop an age-associated obesity. A direct link of Prmt7 to human obesity has not been found; however, a recent genome-wide association study has identified eight single nucleotide polymorphisms in the CTCF-PRMT7 region of the human chromosome 16q22.1 linked to low serum HDL and dyslipidemia (50). In addition, the human chromosomal region 16q22–23 contains genes, such as FTO and MAF, that are associated with obesity (51). A recent study on genes associated with recessive developmental disorders has identified a rare missense mutation in the Prmt7 gene in three families (52). Consistently, Prmt7 mutant mice phenocopy the associated clinical phenotypes, such as pseudohypoparathyroidism and mild intellectual disability, with obesity. This study further support a role of Prmt7 in metabolic control; however, the molecular mechanism underlying such clinical phenotypes is unclear. The whole-body metabolism analysis of Prmt7-deficient mice suggests that the obesity observed in Prmt7-deificent mice likely is linked to the decreased EE. The decrease in oxidative fibers found in TA and EDL muscles of Prmt7-null mice is accompanied by an increased proportion of glycolytic fiber type IIx and IIb at the expense of oxidative fiber type I and IIa. Growing evidence supports that a shift from oxidative to glycolytic muscle metabolism is associated with an imbalance in energy homeostasis and causes exacerbation of diet-induced glucose intolerance, insulin resistance, and obesity in mice (5–8). Furthermore, the proportion of oxidative fibers correlates positively with whole-body insulin sensitivity in humans (19). In obesity and type 2 diabetes, skeletal muscle exhibits a reduced oxidative capacity and increased glycolytic activities. Notably, Prmt7-deficient mice at a young age exhibit the fiber-type switch without any signs of obese phenotypes. Therefore, the fiber-type switch appears to be the cause and not the consequence of obesity in Prmt7-deficient mice.

Consistent with the decreased oxidative metabolism, Prmt7-deficient muscles exhibit decreased expression of various regulatory genes for the oxidative muscle function including PGC-1α and PPARs. The decrease in oxidative metabolism is accompanied by the reduction in mitochondrial contents and the endurance muscle function. Several studies have shown that PGC-1 coactivators play critical roles in the control of muscle oxidative metabolism, mitochondrial biogenesis, and energy homeostasis (9,14,15). The muscle-specific ablation of PGC-1α results in a fiber-type switch toward less oxidative fibers along with impaired endurance exercise and age-associated obesity (16,17). The ability of Prmt7 to regulate the metabolic capacity in skeletal muscle may be achieved, at least in part, through PGC-1α transcription in response to various stimuli like exercise. This is further supported by the fact that Prmt7 depletion in differentiating myoblasts caused decreased expression of PGC-1α and its target genes (Fig. 6). Prmt7 appears to regulate PGC-1α expression through CRE by the activation of ATF2 and p38 without affecting the expression of these genes. Prmt7 can be recruited to the CRE site in the PGC-1α promoter region with ATF2 and pp38. Since Prmt7 interacts with p38, it is possible that Prmt7-mediated methylation of p38 may play a critical role for its activation. A recent study has shown that Prmt1 associates with p38, leading to its methylation and activation required for erythroid differentiation (48). Using an antibody recognizing symmetric dimethylation of arginine (Sym10), we proved that Prmt7 specifically increased the symmetric methylarginine-specific p38 without alteration of Prmt5 levels (Fig. 8*B*). Another possibility is that Prmt7 interacts with active p38 in nucleus and stabilizes the active form, thereby prolonging its downstream events. Depending on cell types or contexts, PGC-1α expression is regulated differentially by distinctive signaling pathways and transcription regulators. For example, FOXO1 and CREB play critical roles in the regulation of PGC-1α expression in hepatic cells, while MEF2c, ATF2, and CREB have been shown to be important in skeletal muscles (13). In support of the differential mode of PGC-1α gene regulation, Prmt7 deficiency did not alter PGC-1α levels in livers of HFD-fed mice, and PGC-1α expression levels were slightly elevated in white adipose tissue from Prmt7-deficient mice (H.-J.L. and J.-S.K., unpublished data). An alternative but not exclusive mechanism is that Prmt7 may activate transcription factors, like MEF2c or MyoD, in addition to PGC-1α through p38/ATF2, which play critical roles in expression of fiber-type switch–related genes. We showed that MEF2c and MyoD were reduced in *Prmt7*$^{-/-}$ mice. This is further supported by the recent studies showing that PGC-1α may be required for exercise-induced mitochondrial biogenesis but not for fiber-type switch (53).

In addition to skeletal muscle, Prmt7 is also expressed in various energy-expanding tissues, including heart and brown adipose tissues. In contrast to skeletal muscle, which developed a fiber-type switch from oxidative to glycolytic muscle at the age of 4 months, however, heart and brown adipose tissues did not show any gross change at the age of 4 months, including organ weights, the size and appearance of adipocytes, and the mitochondrial DNA. Given that decreased EE and exercise capacity were already observed in 4- to 5-month-old *Prmt7*$^{-/-}$ mice (Figs. 3 and 4), the muscle function plays a key role in defective energy metabolism of Prmt7-deficient mice. However, we do not rule out the possible contribution of tissues other than skeletal muscle, and we are currently generating tissue-specific knockout mice to further address the specific contribution of skeletal muscle to this phenotype in future.

In conclusion, the results presented here provide the first direct evidence of functional roles for Prmt7 in the skeletal muscle at the gene expression, muscle fiber-type switch, and

Downloaded from http://diabetesjournals.org/diabetes/article-pdf/65/7/1868/599654/db151500.pdf by guest on 21 April 2025

whole-body metabolism levels. Recent studies have suggested the PGC-1α activation pathway as a therapeutic target to circumvent mitochondrial dysfunction and muscle atrophy in pathological states or normal muscle aging (54,55). Like PGC-1α, Prmt7 appears to be critical for maintenance of muscle mass in aging, and Prmt7-null mice exhibit premature loss of muscle mass. Thus, it is conceivable that modulation of Prmt7 levels in muscle may be an important target to increase mitochondrial biogenesis and to treat muscle atrophy and obesity-related metabolic conditions.

Acknowledgments. The authors thank Drs. Ruth Simon (University of Ulm), Robert S. Krauss (Mount Sinai School of Medicine), and Dario Colleti (Sapienza University of Rome) for critical reading of the manuscript.

Funding. This research was supported by the National Research Foundation of Korea, funded by the Korean Government, Ministry of Science, ICT and Future Planning (NRF-2011-0017315 and NRF-2013M3A9B1069776).

Duality of Interest. No potential conflicts of interest relevant to this article were reported.

Author Contributions. H.-J.J., H.-J.L., T.A.V., K.-S.C., D.C., and S.C.C. contributed to the experimental design, research, and data analysis. S.-H.K., H.C., and J.-S.K. contributed to the experimental design and data analysis. J.-S.K. wrote the manuscript. J.-S.K. is the guarantor of this work and, as such, had full access to all the data in the study and takes responsibility for the integrity of the data and the accuracy of the data analysis.

References

1. Doherty TJ. Invited review: aging and sarcopenia. J Appl Physiol (1985) 2003;95:1717–1727
2. Cohen S, Nathan JA, Goldberg AL. Muscle wasting in disease: molecular mechanisms and promising therapies. Nat Rev Drug Discov 2015;14:58–74
3. Morley JE, Baumgartner RN, Roubenoff R, Mayer J, Nair KS. Sarcopenia. J Lab Clin Med 2001;137:231–243
4. Zierath JR, Hawley JA. Skeletal muscle fiber type: influence on contractile and metabolic properties. PLoS Biol 2004;2:e348
5. Hickey MS, Carey JO, Azevedo JL, et al. Skeletal muscle fiber composition is related to adiposity and in vitro glucose transport rate in humans. Am J Physiol 1995;268:E453–E457
6. Wang YX, Zhang CL, Yu RT, et al. Regulation of muscle fiber type and running endurance by PPARdelta. PLoS Biol 2004;2:e294
7. Mootha VK, Lindgren CM, Eriksson KF, et al. PGC-1alpha-responsive genes involved in oxidative phosphorylation are coordinately downregulated in human diabetes. Nat Genet 2003;34:267–273
8. Oberbach A, Bossenz Y, Lehmann S, et al. Altered fiber distribution and fiber-specific glycolytic and oxidative enzyme activity in skeletal muscle of patients with type 2 diabetes. Diabetes Care 2006;29:895–900
9. Lin J, Handschin C, Spiegelman BM. Metabolic control through the PGC-1 family of transcription coactivators. Cell Metab 2005;1:361–370
10. Scarpulla RC. Transcriptional paradigms in mammalian mitochondrial biogenesis and function. Physiol Rev 2008;88:611–638
11. Yan Z. Exercise, PGC-1alpha, and metabolic adaptation in skeletal muscle. Appl Physiol Nutr Metab 2009;34:424–427
12. Combes A, Dekerle J, Webborn N, Watt P, Bougault V, Daussin FN. Exercise-induced metabolic fluctuations influence AMPK, p38-MAPK and CaMKII phosphorylation in human skeletal muscle. Physiol Rep 2015;3:e12462
13. Fernandez-Marcos PJ, Auwerx J. Regulation of PGC-1α, a nodal regulator of mitochondrial biogenesis. Am J Clin Nutr 2011;93:884S–890S
14. Handschin C, Choi CS, Chin S, et al. Abnormal glucose homeostasis in skeletal muscle-specific PGC-1alpha knockout mice reveals skeletal muscle-pancreatic beta cell crosstalk. J Clin Invest 2007;117:3463–3474
15. Handschin C, Spiegelman BM. Peroxisome proliferator-activated receptor gamma coactivator 1 coactivators, energy homeostasis, and metabolism. Endocr Rev 2006;27:728–735
16. Schuler M, Ali F, Chambon C, et al. PGC1alpha expression is controlled in skeletal muscles by PPARbeta, whose ablation results in fiber-type switching, obesity, and type 2 diabetes. Cell Metab 2006;4:407–414
17. Handschin C, Chin S, Li P, et al. Skeletal muscle fiber-type switching, exercise intolerance, and myopathy in PGC-1alpha muscle-specific knock-out animals. J Biol Chem 2007;282:30014–30021
18. Crunkhorn S, Dearie F, Mantzoros C, et al. Peroxisome proliferator activator receptor gamma coactivator-1 expression is reduced in obesity: potential pathogenic role of saturated fatty acids and p38 mitogen-activated protein kinase activation. J Biol Chem 2007;282:15439–15450
19. Patti ME, Butte AJ, Crunkhorn S, et al. Coordinated reduction of genes of oxidative metabolism in humans with insulin resistance and diabetes: potential role of PGC1 and NRF1. Proc Natl Acad Sci U S A 2003;100:8466–8471
20. Sandri M, Lin J, Handschin C, et al. PGC-1alpha protects skeletal muscle from atrophy by suppressing FoxO3 action and atrophy-specific gene transcription. Proc Natl Acad Sci U S A 2006;103:16260–16265
21. Leone TC, Lehman JJ, Finck BN, et al. PGC-1alpha deficiency causes multisystem energy metabolic derangements: muscle dysfunction, abnormal weight control and hepatic steatosis. PLoS Biol 2005;3:e101
22. Lin J, Wu H, Tarr PT, et al. Transcriptional co-activator PGC-1 alpha drives the formation of slow-twitch muscle fibres. Nature 2002;418:797–801
23. Cao W, Daniel KW, Robidoux J, et al. p38 mitogen-activated protein kinase is the central regulator of cyclic AMP-dependent transcription of the brown fat uncoupling protein 1 gene. Mol Cell Biol 2004;24:3057–3067
24. Akimoto T, Pohnert SC, Li P, et al. Exercise stimulates Pgc-1alpha transcription in skeletal muscle through activation of the p38 MAPK pathway. J Biol Chem 2005;280:19587–19593
25. Wright DC, Han DH, Garcia-Roves PM, Geiger PC, Jones TE, Holloszy JO. Exercise-induced mitochondrial biogenesis begins before the increase in muscle PGC-1alpha expression. J Biol Chem 2007;282:194–199
26. Fan M, Rhee J, St-Pierre J, et al. Suppression of mitochondrial respiration through recruitment of p160 myb binding protein to PGC-1alpha: modulation by p38 MAPK. Genes Dev 2004;18:278–289
27. Olesen J, Kiilerich K, Pilegaard H. PGC-1alpha-mediated adaptations in skeletal muscle. Pflugers Arch 2010;460:153–162
28. Safdar A, Little JP, Stokl AJ, Hettinga BP, Akhtar M, Tarnopolsky MA. Exercise increases mitochondrial PGC-1alpha content and promotes nuclear-mitochondrial cross-talk to coordinate mitochondrial biogenesis. J Biol Chem 2011;286:10605–10617
29. Adhihetty PJ, Uguccioni G, Leick L, Hidalgo J, Pilegaard H, Hood DA. The role of PGC-1alpha on mitochondrial function and apoptotic susceptibility in muscle. Am J Physiol Cell Physiol 2009;297:C217–C225
30. Bedford MT, Clarke SG. Protein arginine methylation in mammals: who, what, and why. Mol Cell 2009;33:1–13
31. Pal S, Sif S. Interplay between chromatin remodelers and protein arginine methyltransferases. J Cell Physiol 2007;213:306–315
32. Migliori V, Müller J, Phalke S, et al. Symmetric dimethylation of H3R2 is a newly identified histone mark that supports euchromatin maintenance. Nat Struct Mol Biol 2012;19:136–144
33. Choi D, Oh KJ, Han HS, et al. Protein arginine methyltransferase 1 regulates hepatic glucose production in a FoxO1-dependent manner. Hepatology 2012;56:1546–1556
34. Tsai WW, Niessen S, Goebel N, Yates JR 3rd, Guccione E, Montminy M. PRMT5 modulates the metabolic response to fasting signals. Proc Natl Acad Sci U S A 2013;110:8870–8875
35. Teyssier C, Ma H, Emter R, Kralli A, Stallcup MR. Activation of nuclear receptor coactivator PGC-1alpha by arginine methylation. Genes Dev 2005;19:1466–1473

Downloaded from http://diabetesjournals.org/diabetes/article-pdf/65/7/1868/599654/db151500.pdf by guest on 21 April 2025

36. Chen SL, Loffler KA, Chen D, Stallcup MR, Muscat GE. The coactivator-associated arginine methyltransferase is necessary for muscle differentiation: CARM1 coactivates myocyte enhancer factor-2. J Biol Chem 2002;277:4324–4333

37. Dacwag CS, Bedford MT, Sif S, Imbalzano AN. Distinct protein arginine methyltransferases promote ATP-dependent chromatin remodeling function at different stages of skeletal muscle differentiation. Mol Cell Biol 2009;29:1909–1921

38. Kawabe Y, Wang YX, McKinnell IW, Bedford MT, Rudnicki MA. Carm1 regulates Pax7 transcriptional activity through MLL1/2 recruitment during asymmetric satellite stem cell divisions. Cell Stem Cell 2012;11:333–345

39. Zhang T, Günther S, Looso M, et al. Prmt5 is a regulator of muscle stem cell expansion in adult mice. Nat Commun 2015;6:7140

40. Kwon YR, Jeong MH, Leem YE, et al. The Shh coreceptor Cdo is required for differentiation of midbrain dopaminergic neurons. Stem Cell Res (Amst) 2014;13:262–274

41. Bae GU, Lee JR, Kim BG, et al. Cdo interacts with APPL1 and activates Akt in myoblast differentiation. Mol Biol Cell 2010;21:2399–2411

42. Tran P, Ho SM, Kim BG, et al. TGF-β-activated kinase 1 (TAK1) and apoptosis signal-regulating kinase 1 (ASK1) interact with the promyogenic receptor Cdo to promote myogenic differentiation via activation of p38MAPK pathway. J Biol Chem 2012;287:11602–11615

43. Jeong MH, Ho SM, Vuong TA, et al. Cdo suppresses canonical Wnt signalling via interaction with Lrp6 thereby promoting neuronal differentiation. Nat Commun 2014;5:5455

44. Lee HJ, Bae GU, Leem YE, et al. Phosphorylation of Stim1 at serine 575 via netrin-2/Cdo-activated ERK1/2 is critical for the promyogenic function of Stim1. Mol Biol Cell 2012;23:1376–1387

45. Kang JS, Yi MJ, Zhang W, Feinleib JL, Cole F, Krauss RS. Netrins and neogenin promote myotube formation. J Cell Biol 2004;167:493–504

46. Lee JM, Seo WY, Song KH, et al. AMPK-dependent repression of hepatic gluconeogenesis via disruption of CREB.CRTC2 complex by orphan nuclear receptor small heterodimer partner. J Biol Chem 2010;285:32182–32191

47. O'Hagan KA, Cocchiglia S, Zhdanov AV, et al. PGC-1alpha is coupled to HIF-1alpha-dependent gene expression by increasing mitochondrial oxygen consumption in skeletal muscle cells. Proc Natl Acad Sci U S A 2009;106:2188–2193

48. Hua WK, Chang YI, Yao CL, Hwang SM, Chang CY, Lin WJ. Protein arginine methyltransferase 1 interacts with and activates p38α to facilitate erythroid differentiation. PLoS One 2013;8:e56715

49. Kanade SR, Eckert RL. Protein arginine methyltransferase 5 (PRMT5) signaling suppresses protein kinase Cδ- and p38δ-dependent signaling and keratinocyte differentiation. J Biol Chem 2012;287:7313–7323

50. Aulchenko YS, Ripatti S, Lindqvist I, et al.; ENGAGE Consortium. Loci influencing lipid levels and coronary heart disease risk in 16 European population cohorts. Nat Genet 2009;41:47–55

51. Hofker M, Wijmenga C. A supersized list of obesity genes. Nat Genet 2009;41:139–140

52. Akawi N, McRae J, Ansari M, et al.; DDD study. Discovery of four recessive developmental disorders using probabilistic genotype and phenotype matching among 4,125 families. Nat Genet 2015;47:1363–1369

53. Geng T, Li P, Okutsu M, et al. PGC-1alpha plays a functional role in exercise-induced mitochondrial biogenesis and angiogenesis but not fiber-type transformation in mouse skeletal muscle. Am J Physiol Cell Physiol 2010;298:C572–C579

54. Dillon LM, Rebelo AP, Moraes CT. The role of PGC-1 coactivators in aging skeletal muscle and heart. IUBMB Life 2012;64:231–241

55. Wenz T, Rossi SG, Rotundo RL, Spiegelman BM, Moraes CT. Increased muscle PGC-1alpha expression protects from sarcopenia and metabolic disease during aging. Proc Natl Acad Sci U S A 2009;106:20405–20410

Downloaded from http://diabetesjournals.org/diabetes/article-pdf/65/7/1868/599654/db151500.pdf by guest on 21 April 2025